SUSTAINED GLIDER OBSERVATIONS OF ACOUSTIC SCATTERING SUGGEST ZOOPLANKTON PATCHES ARE DRIVEN BY VERTICAL MIGRATION AND SURFACE ADVECTIVE FEATURES IN PALMER CANYON, ANTARCTICA

by

Cordielyn S. Goodrich

A thesis submitted to the Faculty of the University of Delaware in partial fulfillment of the requirements for the degree of Master of Science in Marine Studies

Spring 2018

© 2018 Cordielyn S. Goodrich
All Rights Reserved

SUSTAINED GLIDER OBSERVATIONS OF ACOUSTIC SCATTERING SUGGEST ZOOPLANKTON PATCHES ARE DRIVEN BY VERTICAL MIGRATION AND SURFACE ADVECTIVE FEATURES IN PALMER CANYON, ANTARCTICA

by

Cordielyn S. Goodrich

Approved: _____
Matthew J. Oliver, Ph.D.
Professor in charge of thesis on behalf of the Advisory Committee

Approved: _____
Mark A. Moline, Ph.D.
Director of the School of Marine Science and Policy

Approved: _____
Estella Atekwana, Ph.D.
Dean of the College of College of Earth, Ocean, and Environment

Approved: _____
Ann L. Ardis, Ph.D.
Senior Vice Provost for Graduate and Professional Education

ACKNOWLEDGMENTS

I am so fortunate to have gotten to spend a couple years at the University of Delaware, College of Earth, Ocean, and Environment, the community and people there are truly second to none. I am so thankful to have gotten to work with my advisor Matt Oliver. He is not only an amazing scientist but also one of the kindest and most caring individuals that I have ever met. Matt was encouraging, inspiring, and a wonderful teacher. He always made me feel comfortable and at home during my time in his lab. Not to mention we have a lot in common, for example, we both can be caught lying about how long it's been since we've eaten a doughnut! I am also grateful for the guidance provided my committee members, Josh Kohut from Rutgers and Jon Cohen. I learned a lot from both Josh and Jon, they provided really helpful feedback and insight to this project. I am thankful for the funding I received during this project provided by NSF.

The staff at CEOE including, Lisa Dorey, Luci Coumatos, and Carol Kitchen, are awesome! A special thanks to Janis, I could not have finished this project without her support. She is encouraging, kind, and goes above and beyond to help with any problem, big or small. Megan Cimino was an excellent mentor during the course of this project. I am grateful for her insight on the Antarctic ecosystem and the kindness and patience she showed while helping me work through difficult concepts.

My labmates played a huge role in my graduate school career. They were extremely supportive and made my time in this program a really positive experience, full of laughs and really fond memories. Danielle Haulsee and Matt Breece were great

role models for me. They lead by example and taught me countless things about gliders, coding, statistics, dark chocolate, and snapchat filters. Their ideas and criticism strengthened this project dramatically. I continue to aspire to be like them. Joe Gradone put a smile on my face every day and is the definition of a teammate. From building a wooden box to running a race (I was always faster), Joe and I can get anything done together. Although we only overlapped for a short period, Katie Hudson's enthusiasm is second to none. Thankful that my labmates put up with my eye rolling and handstands and always made me feel like the queen!

I am truly lucky to have the most supportive family and friends. I will never be able to thank my mom, Michelle, enough. She encourages me in everything I do, pushes me to pursue my passions, and from a young age stressed the value of education. My sister, Lee, and the rest of my family have shown me so much love and support. I have many friends that have helped me through this process. In particular, Tim Pilegard, Lane Johnston, and Jason Button were key players; these three helped me succeed and also helped me keep smiling through the challenges. Thankful for all that listened to both my excitement and frustrations during this project. I feel so loved and lucky, I am so grateful for that!

TABLE OF CONTENTS

LIST OF TABLES

LIST OF FIGURES

ABSTRACT

Antarctic zooplankton and micronekton link the highly productive waters of the Southern Ocean to upper trophic levels. The distribution of zooplankton and micronekton is highly patchy both vertically and horizontally, suggesting that both behavior and oceanographic advection are important for understanding their distributions. A Slocum glider was deployed with an acoustic Doppler current profiler within a surface current field measured by HF-Radar in Palmer Canyon, Antarctica, during austral summer. I used this data to investigate the relative importance of surface currents and vertical migration behavior on the presence of zooplankton and micronekton in the mixed layer. I show that zooplankton and micronekton are more likely to be found shallower than the mixed layer during night-time hours, indicating diel vertical migration is a driver of their vertical distribution. I also found both Eulerian and Lagrangian characterizations of surface physical features to be important in predicting the presence of zooplankton and micronekton shallower than the mixed layer. While I found that both diel vertical migration (DVM) and surface currents were significant predictors of zooplankton and micronekton presence above the mixed layer, the strongest predictor of zooplankton and micronekton presence were surface currents represented as repelling Lagrangian Coherent Structures (LCS). This indicates that in this region during summer, horizontal advection and behavior plays a critical component in structuring zooplankton and micronekton distributions.

Chapter 1

INTRODUCTION

Zooplankton and micronekton are spatially heterogeneous and "patchy" across multiple spatial scales (Pinel-Alloul 1995) and occupy intermediate Reynolds numbers (10^{-2}-10^{3}) (Catton et al. 2011; Yen 2000). This means that both advection and swimming behavior likely shape zooplankton and micronekton patches, making the factors driving their distribution difficult to uncover. However, because zooplankton and micronekton are a critical trophic link between primary producers and upper trophic levels, understanding the factors driving their distribution is critical, especially in trophically short polar food webs. Krill, salps, and copepods are the dominant zooplankton and micronekton (from here forward I will refer broadly to zooplankton and micronekton communities as "zooplankton") in Antarctica (Smith et al. 1995). However, their diversity and abundance varies greatly between areas (Schnack-Schiel & Mujica 1994). For example, Chojnacki & Węgleńska (1984) showed that copepods dominated summer zooplankton biomass in Admiralty Bay. Zhou et al. (1994) found that krill were the primary zooplankton taxa in the Gerlache Strait. On daily time scales, Antarctic zooplankton participate in diel vertical migration (DVM). They occupy shallower depths during the night and sink deeper during the day to maximize feeding efforts and avoid predation from visual predators (Cohen & Forward 2009). Vertical distribution of zooplankton also varies seasonally. For some copepods abundance increases near the surface during the summer (Atkinson 1998; Lawson et al. 2004; Smith et al. 1995). Similarly, an increase in krill abundance was found

during the spring and summer on the West Antarctic Peninsula (Lascara et al. 1999). Horizontal distribution of zooplankton is also often influenced by surface currents. For example, (Lawson et al. 2004) observed changes seasonally in zooplankton biomass that they attributed to high zooplankton association with a gyre and coastal current. However, studies that estimate the relative importance of behavior and advection on zooplankton distributions are rare (Folt and Burns, 1999).

Palmer Canyon, Antarctica supports enhanced phytoplankton production (Kavanaugh et al. 2015) and is considered a biological hotspot that is home to Adélie (*Pygoscelis adeliae*), gentoo (*P. papua*) and chinstrap (*P. antarcticus*) penguins (Emslie et al. 1998). This region is also a common feeding ground for Humpback whales (*Megaptera novaeangliae*) (Friedlaender et al. 2008) indicating that it is a persistent place where zooplankton link primary producers to upper trophic levels. In the Palmer Long Term Ecological Research region euphausiids (*Euphausia superba*, Antarctic krill; *Thysanoëssa macrura*; *Euphausia crystallorophias*, ice krill), a shelled pteropod (*Limacina helicina*), and a salp (*Salpa thompsoni*) numerically dominate the macro- and mesozooplankton communities (Ross et al. 2008). In the nearby Marguerite Bay area, krill and copepods were the domination zooplankton in the fall in both biomass and abundance (Ashjian et al. 2004). Previous studies have shown that strong zooplankton acoustic signals are associated with the depth of the chlorophyll maximum, lower integrated surface chlorophyll, and low light levels – all indicating a strong coherence to the vertical structure of the water column (Cimino et al. 2016). However, less is known about what drives horizontal heterogeneity of Antarctic zooplankton, including krill. Bernard & Steinberg (2013) compared krill biomass near the head of the canyon during diurnal and semidiurnal tidal regimes and found that

during diurnal tides, krill biomass was significantly higher. A similar study found that krill were influenced by tidal regime and wind; with diurnal tides and predominant westerly winds resulting in higher krill abundance (Bernard et al. 2017). This inferred horizontal pattern in krill distribution is supported by changes in Adélie penguin locations based on tidal regime (Oliver et al. 2013). During diurnal tides, Adélie penguins foraged inshore, and moved more offshore during semi-diurnal tides. These studies suggest that nearshore regions of the Palmer biological hotspot may be supported by advective features that concentrate otherwise disperse aggregations of krill and other zooplankton. Little is known about the advective mechanisms that influence the horizontal distribution of these organisms, or how important they are relative to the mechanisms driving their vertical distribution.

Areas of divergence (upwelling) and convergence (downwelling) are features in the fluid environment often associated with zooplankton concentrations or community structure. These areas give a Eulerian perspective of the hydrography that zooplankton encounter. Many studies have shown zooplankton association with these features (Simard et al. 1986; Paffenhofer, 1980; Wishner et al. 1995). For example, Croll et al. (2005) shows that euphausiids are spatially associated with wind driven upwelling areas. In the northern Bering Sea, Russell et al (1999) hypothesized that convergence at a front and subsurface advection are responsible for concentrations of copepods and euphausiids respectively.

An alternative to using the Eulerian perspective to understand the physical oceanography is to use the Lagrangian perspective. Lagrangian Coherent Structures (LCS) are special surfaces of fluid trajectories that organize the surrounding flow into ordered patterns (Haller 2015). They are structures that influence the trajectory of fluid

parcels that often create transport barriers across which movement of particles is difficult. These structures are often associated with mesoscale features such as filaments and fronts. LCS features can be classified as either attractive (aLCS) or repelling (rLCS) based on passive particle trajectories. Particle trajectories move along and toward an aLCS material line and along and away from a rLCS material line. In the California current system, both aLCS and rLCS had higher particle concentrations than the background, but that most particles were located along aLCS features (Harrison et al. 2013). It is important to note that since LCS structures are computed as particle tracers in a 2D field, aLCS and rLCS are not synonyms for convergence and divergence, which imply vertical velocities. Rather particles associated with aLCS are considered confluent, while particles associated with rLCS are considered diffluent (Harrison et al. 2013).

The inferred particle behaviors associated with LCS structures in the ocean are potentially interesting ecological cues. If these features influence or control the distribution of low Reynolds number (10^{-4}-10^{3}) organisms such as phytoplankton, zooplankton, or other prey, they may act as dynamic attractors for top predators. Indeed, LCS have been utilized in a number of recent studies looking at the potential impact of ocean circulation on phytoplankton measured by satellite ocean color in the open ocean (d'Ovidio et al. 2010), and krill estimated from acoustic transects in the Gulf of St. Lawrence (Maps et al. 2015). Furthermore, organisms dependent on these plankton may also be collocated with LCS features including Great Frigatebird (*Fregata minor*) (Tew Kai et al. 2009), Fin whales (*Balaenoptera physalus*) (Cotte et al. 2011) and Southern Elephant seals (*Mirounga leonine*) (Della Penna et al. 2015). Each of these studies showed organismal associations with aLCS features over

relatively large scales O(100 km). The explanations given for these associations were the attractive nature of the aLCS on potential prey items. However only one of these studies (Tew Kai et al. 2009) examined both aLCS and rLCS structures as potential predictors for these organisms, even though both aLCS and rLCS have been shown to be particle associated in simulations (Harrison et al. 2013). The Great Frigatebird was associated with both aLCS and rLCS (Tew Kai et al. 2009) suggesting that both could be important predictors of organismal distributions.

To understand the potential impact of both horizontal and vertical factors influencing zooplankton distributions in Palmer Canyon, which serve as important prey in the region, I analyzed acoustic scatter signals measured by an acoustic Doppler current profiler mounted on an autonomous glider nested within a horizontal current field measured by HF-Radar. I match these observations to derived Eulerian and Lagrangian features from this current field to understand their potential impact on the distribution of zooplankton.

Chapter 2

MATERIALS AND METHODS

2.1 Slocum Glider

An electric Slocum glider (Teledyne Webb Research) was deployed in Palmer Canyon, Western Antarctic Peninsula, on January 5, 2015, recovered to replace batteries for one day on January 21, 2015 and redeployed until February 15, 2015. The Slocum glider is a buoyancy-driven autonomous underwater vehicle that undulates through the water column at ~ 25° angle reaching depths of ~100 m before returning to the surface. Communication with the glider was by iridium satellite phone and location of the glider is attained by GPS. The glider was equipped with a Seabird CTD and a Wetlabs EcoPuck optical sensor that collect continuous measurements of temperature, conductivity, pressure, and chlorophyll fluorescence as the glider travels through the water. Mixed layer depth was computed using maximum buoyancy frequency using the method of (Carvalho et al. 2017). During the deployment in Palmer Canyon the glider spent a total of 21 days station keeping, profiling up and down in one location. This is the time period focused on for the purpose of this study (Figure 2.1).

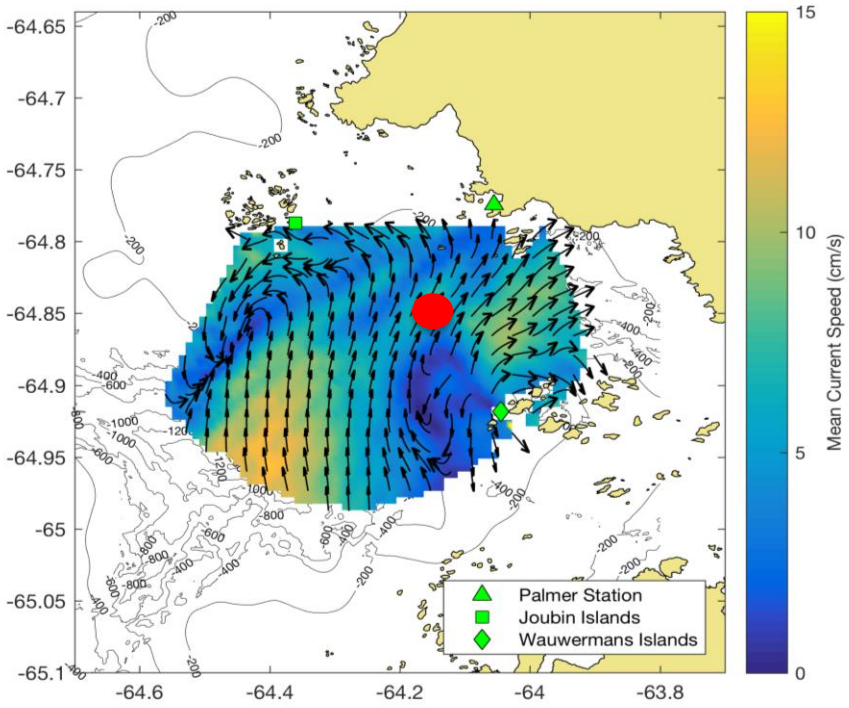

Figure 2.1: A map of Palmer Canyon with the mean current speed and direction (indicated by the black arrows) calculated by the High Frequency Radar from January 12- February 5, 2015. The red point indicates the location where the glider profiled with the ADCP. The green triangle, square, and diamond indicated where the three HFR stations were located.

An upward looking 1 MHz acoustic Doppler current profiler (Nortek Aquadopp) was also mounted on top of the glider to collect acoustic backscatter measurements used as a proxy for the presence of zooplankton scatters in the water column (Brierley et al. 1998; Roe & Griffiths 1993). The face of the ADCP was angled at 25° to compensate for the glider dive angle. As the glider dove, the face of

the ADCP was looking upward approximately perpendicular with the surface of the water (Figure 2.2). The ADCP recorded acoustic backscatter along 3 beams in 1 m vertical bins at 0.5 Hz. The acoustic bin 4 m from the glider was used to assess presence-absence of acoustic scatters, following the approach by (Baumgartner & Fratantoni 2008). The putative particle diameters detected by this frequency are greater than ~ 640 µm (Lohrmann 2001). Since the Aquadopp is mounted to operate perpendicular to the surface of the water for the glider descent, the beam orientation shifts to be more horizontal during the glider ascent. Therefore the absolute depth of the measurement (bin 4) during ascent relative to the glider must be corrected for this change in orientation. The following equations are used to calculate the correction applied to the Aquadopp depth measurements during glider ascent.

$$\cos(P) * B = Z \quad (1)$$

$$Z - B = C \quad (2)$$

where *P* is the pitch of the glider, *B* is the bin height, *Z* is the number of meters above the glider that the Aquadopp measurement is being taken, and *C* is the depth correction to match with the glider depth measurements.

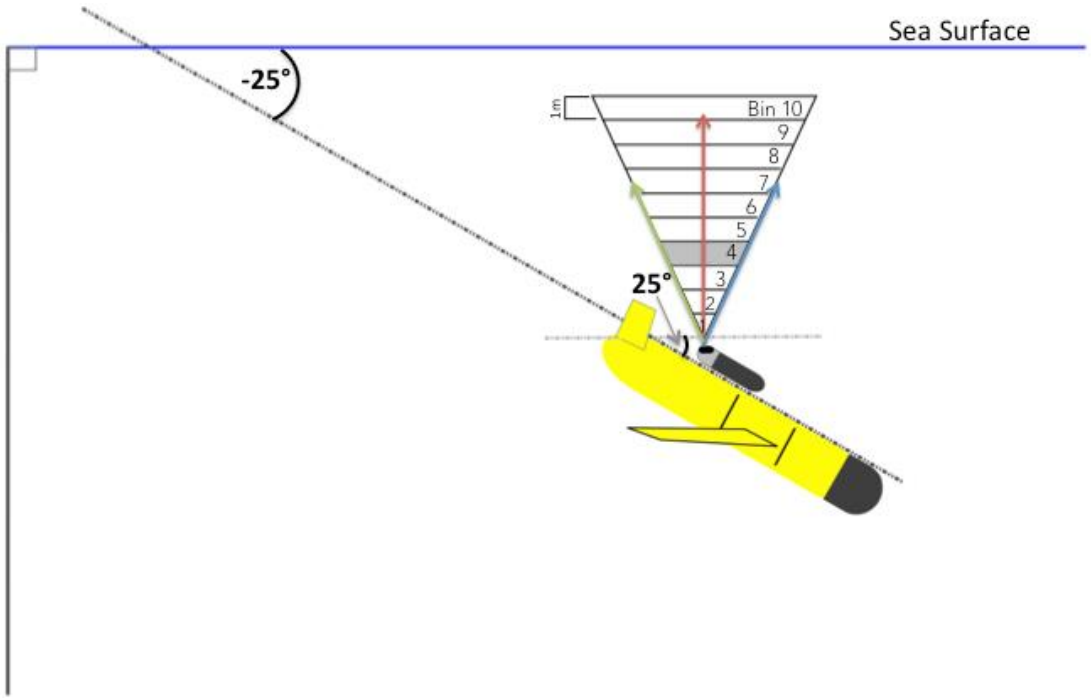

Figure 2.2: The ADCP was mounted up-ward looking on top of the glider. The face of the ADCP was tilted 25° to account for the glider dive angle. As the glider descended the ADCP measured ten 1 m bins directly above it, roughly perpendicular to the sea surface. This design resulted in a miscalculation of depth by the ADCP during glider ascent, which we corrected for.

The ADCP and glider were not integrated, so they each recorded depth and time separately. The glider clock was used as the reference clock. The acoustic data was matched to the glider data based on inflections and profile number. A profile is defined as a half of one full undulation of the glider, marked by a depth inflection on either side. Consecutive measurements collected from both instruments were grouped into 1 m depth bins and averaged. For this study, I focused on the strongest acoustic scattering data, assuming these signals were likely Antarctic krill or other forage species, to indicate either their presence or absence. To isolate these signals, I used an

acoustic threshold (dB) that varied by depth. This was to account for the shifting acoustic noise floor in the data. Additionally, the upper 10 meters of the water column were excluded due to high surface noise, likely a result of bubble injection due to rough sea states (Melville 1996). A ten-meter depth window was used to assign each depth a threshold value to determine the presence or absence of strong acoustic scatter signals. For a given depth in the water column all of the acoustic values from depths 4 m above and those from 5 m below were grouped together in one distribution. I computed our presence and absence definition for three percentile thresholds, the 91st, 95th, and 99th. The values above the threshold were labeled as presence and values below were labeled as absence. This produced three different estimates of the presence and absence of strong acoustic scattering signals. I used these three thresholds to determine if our results were sensitive to the threshold I selected.

2.2 High Frequency Radar

A three-site high-frequency radar (HFR) network was set up to measure sea-surface currents over Palmer Canyon from November 2014 through March 2015. One HFR site was deployed at Palmer Station, another in the Joubin Islands, and the last in Wauwermans Islands. The Palmer site was powered by Palmer station while the other two sites used remote power systems. Communication with the three sites was possible via Freewave radio modem (Kohut et al., 2014). HFR emits radio waves (3 ~ 30 MHz) and analyses the reflection of the waves off of the ocean surface using Bragg scattering. HFR looks for a Doppler shift in the returning radio waves to determine the radial velocity component of the sea surface wave. The measurements from at least two HFR sites must be integrated to obtain the total velocity vector for the target

(Barrick et al. 1977, Paduan & Graber 1997). The combination of the three HFR sites over Palmer canyon provides a 1,500 km^2 surface current map with 0.5 to 1 km resolution every hour during our study.

2.3. Surface Eulerian Features

Surface divergence (represented as vertical velocity at 1 m depth) was calculated using the finite difference method after (Dzwonkowski et al. 2010; Gong et al. 2010; Palamara et al. 2012). A 12 hour 'divergence trend' was calculated to estimate a persistence of divergence in the HF radar field. Values of −1 were assigned to instantaneous divergence (vertical velocity) that were less than -0.1 m d^{-1} (downwelling), 0 to divergence values between -0.1 and $+0.1$ m d^{-1} (neutral) and +1 to divergence values greater than $+0.1$ m d^{-1} (upwelling). Divergence trend has been shown to be an important predictor of fish presence in coastal systems (Palamara et al. 2012).

2.4 Lagrangian Coherent Structures

Finite Time Lyapunov Exponents (FTLE) were used estimate the strength and identify aLCS and rLCS features in the hourly current maps produced by the HF-Radar. FTLE quantifies the strength of surface features over Palmer Deep sampled by the HF radar network. FTLE is calculated based on the fate of simulated particles released in the HFR footprint and tracked over time. The FTLE surfaces quantify the exponential rate at which neighboring particles attract or repel with respect to each other.

The flow map was defined using the following equations:

$$\phi_{t_0}^{T}(x_0) = x_0 + \int_{t_0}^{t_0+T} v(x(t),t)dt \quad (3)$$

$$\phi_{t_0}^{T}(x_0) = x_0 + \int_{t_0}^{t_0-T} v(x(t),t)dt \quad (4)$$

Where the initial position of a particle is defined by x_0, initial time was represented by t_0, T was the length of time over which the integration took place, and ϕ was the flow map. Positive T indicates calculation of the forward FTLE (indicative of repelling particles, equation 3) and negative T indicates calculation of the backward FTLE (indicative of attracting particles, equation 4). FTLE was based on particles simulation on an 800m x 800m grid over the HFR footprint with each grid cell containing 25 Lagrangian particles. The particles in the grid were initialized at time t_0 and advected based on a 3rd order interpolation of the HFR surface current measurements with a 4th-order Runge-Kutta integration for $T = t - t_0$ or $-T = t_0 - t$. This process was performed during twice each day of our study, starting at 00:00 and 12:00 GMT for forward and backward FTLE, and run for 12 hours (T=12 hours). A twelve-hour integration was an adequate time interval to avoid analysis of inconsequential dynamics measured in the fine scale (1 hr) surface currents produced by HFR yet short enough to avoid the advection of a large number of the simulated particles out of the HFR footprint, a result of the rapid currents in Palmer Canyon (Kohut et al. 2018). The gridded Lagrangian trajectory data was compiled into a grid-to-grid transition matrix to identify dominant singular vectors in this matrix and compute FTLE. Since the FTLE calculation represents a time-integrated result every 12 hours, I matched glider profile times in the last three hours of the forward FTLE simulation (9-12Z and 21-24Z) and the first three hours of the backward FTLE simulation (0-3Z and 12-15Z) to the FTLE values. Additionally, to identify likely aLCS and rLCS ridges, I thresholded FTLE values above and below the 50 percentile

of FTLE values. Backward FTLE values larger than the 50^{th} percentile were considered aLCS structures, and forward FTLE values larger than the 50^{th} percentile were considered rLCS structures.

2.5 Tidal Phase Classification

The diurnal and semi-diurnal tidal phase classification followed Oliver at al, 2013. A tide gauge mounted on the pier at Palmer Station, Anvers Island, Antarctica, recorded tidal amplitude during our experiment. Tidal phase classification was based on counting the number of high tides in a day. Time periods with one high tide per day were classified as a diurnal regime and all other tidal time periods were classified as a semidiurnal regime.

2.6 Analysis

Although the frequency of the Aquadopp is similar to frequencies used to detect putative krill swarms in this study area (Cimino et al. 2016), the Aquadopp is not tuned specifically for Antarctic krill. Zooplankton, including krill, are highly patchy, and glider profiles are relatively infrequent. Because of this I was hesitant to use this data to interpret zooplankton or krill aggregation characteristics. Instead I focused on the presence or absence of high acoustic scatterers as likely zooplankton presences (LZPs) above the mixed layer, acknowledging that krill may make up a significant, but unknown, fraction of the detection signal. I analyzed the presence and absence data by profile, above the mixed layer. This was compared to tidal regime, sun angle, average chlorophyll above the mixed layer, average temperature shallower than the mixed layer and advective parameters derived from the HF radar data.

Eulerian metrics for the HF radar data included instantaneous divergence and divergence trend. Lagrangian metrics for the HF radar data included forward and backward FTLE, and thresholded forward and backward FTLE values as indicators of rLCS and aLCS. Our models were binomial generalized linear mixed model (GLMM) with glmer in the R lmerTest package (Kuznetsova et al. 2016). Conditional R^2 values, which include both fixed and random effects, were computed using the r.squaredGLMM function in the R MuMIn package (Bartoń 2017). I used day of year as a random effect to control for variation between days, following (Cimino et al. 2016). One-sided Kolmogorov-Smirnov tests were also used to assess the difference between the distribution of LZPs in daytime and nighttime profiles, and for comparing distributions of advective metrics for profiles with and without LZPs above the mixed layer using the ks.test in the R stats package (R Core Team 2017).

Chapter 3

RESULTS

3.1 Glider Deployments

The glider completed 3,320 profiles during the two station keeping time periods. The glider profiled to 100 m during the first deployment and 90 m for the second deployment. The acoustic return from the ADCP ranged from 21 dB to 59 dB. The thresholds for determining LZPs were depth dependent to account for changing noise floors with depth. As an example, Figure 3.1 shows the distribution of acoustic return at 30 m, 60 m and 90 m with the vertical lines representing the 91st, 95th, and 99th percentiles. Values above these thresholds were considered presences, and values below these thresholds were considered absences. High acoustic returns make up a small percent of the data collected, corroborating the reasoning that the high returns are indicative of spatially heterogeneous scatters such as Antarctic zooplankton.

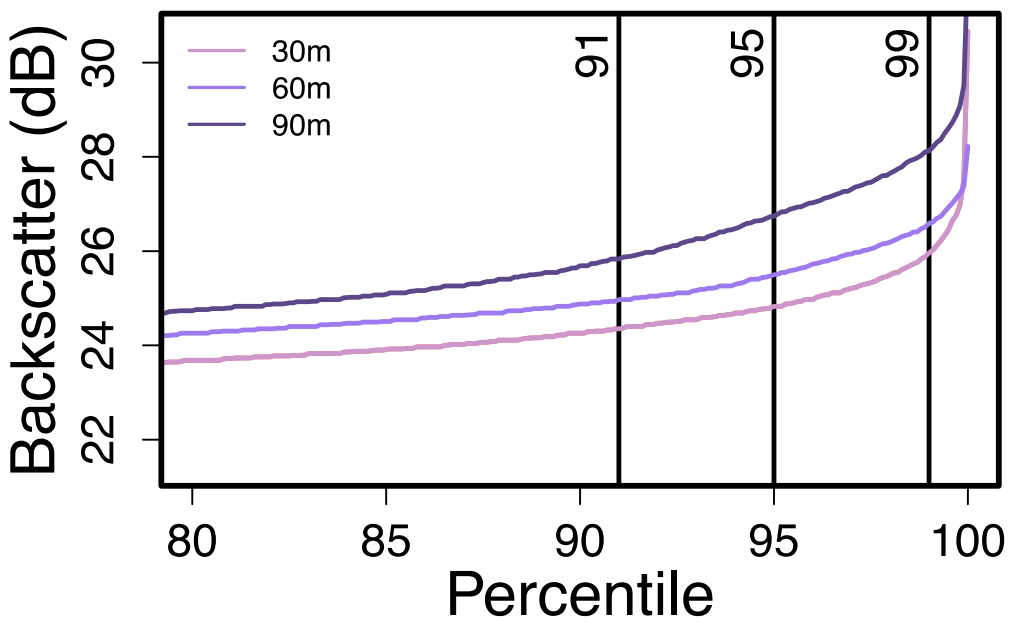

Figure 3.1: Distribution of acoustic backscatter collected from the 30 m, 60 m, and 90 m depth bins. The three vertical lines indicate the three thresholds (91st, 95th, and 99th percentiles) used to classify presence or absence of the LZPs. This serves as an example of how we labeled presence and absence in the acoustic data for each depth using a 10m window. There was very little variation in the majority of the acoustic data. Through this thresholding method we aim to identify data with high acoustic return.

LZPs were distributed throughout the entire glider sampling range. Many presences were found in large groups suggestive of a continuous aggregation of scatters being detected, while others were highly localized. Because the profiling cycle time of the glider was ~20 min, I was hesitant use this data to infer patch morphology over multiple profiles. Figure 3.2 shows wind collected at Palmer Station along with temperature and chlorophyll collected by the glider during the two station keeping time periods, the black points are presences defined by at the 95th percentile, and the

gray circles mark the mixed layer depth (MLD) defined by estimating the maximum buoyancy frequency following the methods of (Carvalho et al. 2017). The MLD is well visualized by the transition from the seasonally warmed surface layer to the depth of the winter water layer (~ -1 C). Between the first and second deployment, Wind velocities between these two time periods approximately doubled, the mixed layer depth deepened from ~ 15 m to ~ 35 m, and chlorophyll concentrations were diluted through the mixed layer (Figure 3.2).

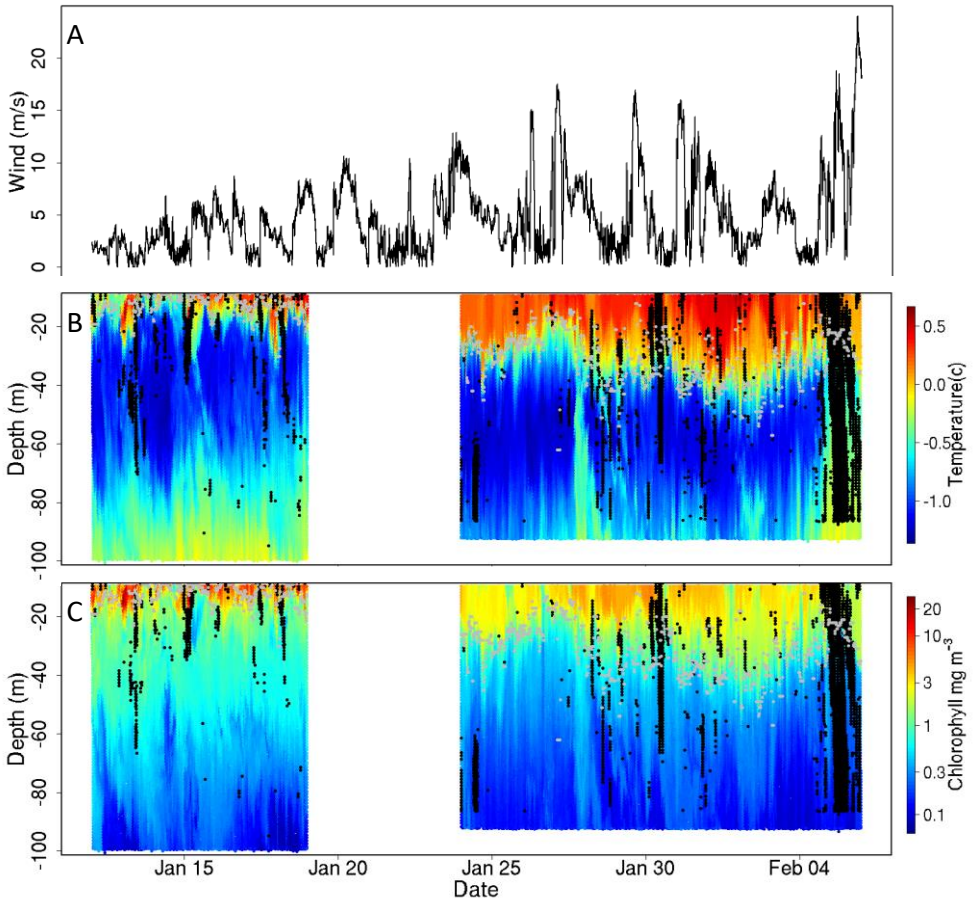

Figure 3.2: (A) Two-minute average wind speed recorded with a digital recording anemometer at Palmer Station. A time series of temperature (B) and chlorophyll (C) collected by the glider, the gray points represent the depth of the mixed layer defined by maximum buoyancy frequency described in Carvalho et al. 2017, the black points are LZPs at the 95th percentile. The missing data in the temperature and chlorophyll time series represents the time that the glider batteries were changed and time spend traveling back to the study site. The mixed layer deepened after the battery change as a result in increased wind speeds.

3.2 Diel Vertical Migrations

Since Antarctic zooplankton are known to perform diel vertical migrations (DVM), I expected that the LZPs would show a diurnal signal. To test this, I compared

the vertical distribution of LZPs during the day (4 hour time window around local noon) to those at night (4 hour time window around local midnight). Figure 3.3 compares the vertical distribution of LZPs during the day to those at night for the three percentile thresholds described above. Nighttime distributions were weighted more heavily toward the surface as expected for a community undergoing DVM. A one-sided Kolmogorov-Smirnov test showed that LZPs were significantly closer to the surface at night for the 91^{st} ($p = << 0.001$, D statistic = 0.056) 95^{th} ($p = << 0.001$, D statistic= 0.113) and 99^{th} ($p = << 0.001$, D statistic= 0.285) percentiles. Only the nighttime distributions of the 91^{st} and the 95^{th} thresholds were not significantly different in a two-sided Kolmogorov-Smirnov test ($p > 0.05$). All other DVM distributions were significantly different from each other ($p < 0.01$).

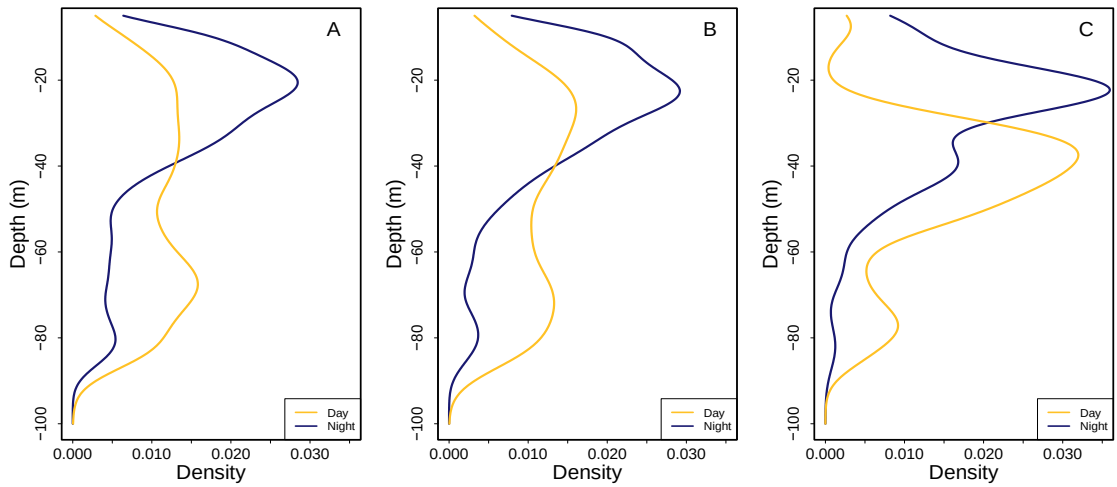

Figure 3.3: Density of LZP observations at night (four hours around local midnight) compared to density of LZP observations during the day (four hours around local noon) for thresholds calculated using the (A) 91st, (B) 95th, and (C) 99th percentiles. For all three thresholds the observations of LZPs at night are concentrated between 10 and 30 m. In contrast, the observations of LZPs during the day are more broadly dispersed with a subtle bimodal distribution. The contrast between the two distributions suggests the LZPs are participating in diel vertical migration.

3.3 Tidal Phases

Of the station keeping time periods, 833 of the 3320 profiles occurred during a diurnal tide. The other 2487 occurred during semidiurnal tides. For the 91st, 95th, and 99th percentile, 33.5%, 19.1%, 5.2% of the profiles during diurnal tides respectively had at least one LZP shallower than the MLD while only 22.4% 14.6%, 3.8% of the semidiurnal profiles had at least one LZP shallower than the MLD respectively (Figure 3.4). A generalized linear model with a binomial response showed that diurnal tides had significantly more LZPs at the 91st ($p << 0.001$, $z = -5.86$) and 95th ($p = 0.004$, $z = -2.85$) LZP percentile thresholds, but not at the 99th LZP percentile threshold ($p = 0.12$, $z = -1.56$).

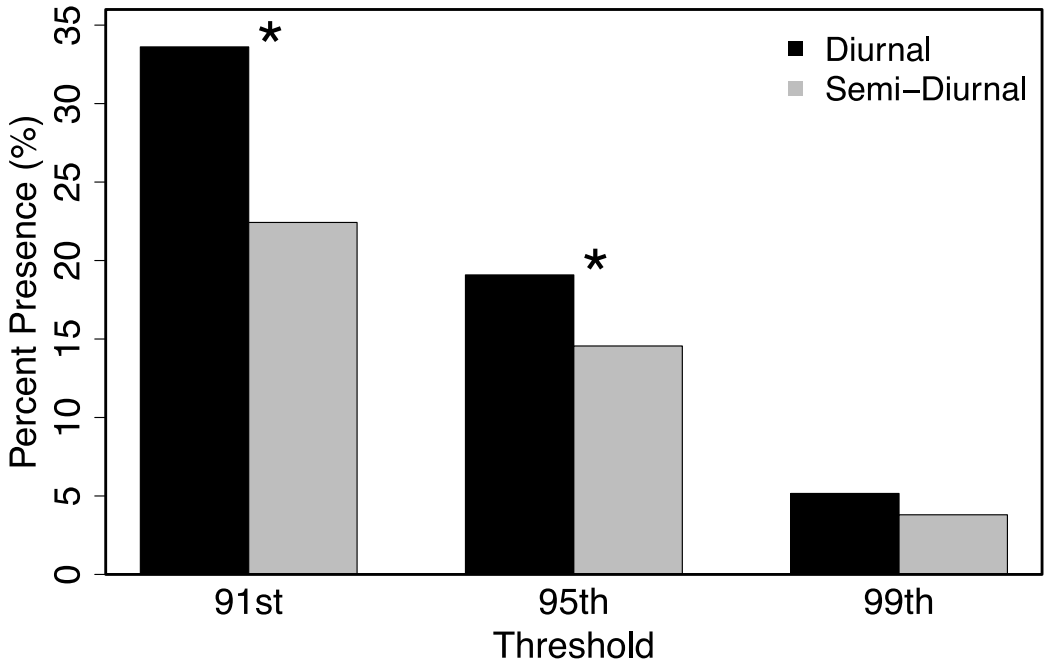

Figure 3.4: Percent of measurements above the mixed layer that are LKPs during the diurnal tidal phase compared to the percent of measurements above the mixed layer that are LKPs during the semi-diurnal tidal phase. For all three thresholds there was a higher percent of presences found during diurnal tide than during semi-diurnal tide. The asterisks indicate significance in the logistic regression.

3.4 LZPs with Eulerian metrics

Hourly divergence and divergence trend were matched to each glider profile (3,320). Of these profiles 663, 411, and 106 of them had LZPs above the MLD for the 91st, 95th, and 99th percentile threshold, respectively. To compare the effect divergence and divergence trend had on LZPs shallower than the MLD, I performed a

Kolmogorov-Smirnov test between all divergence and divergence trend values matched to station keeping profiles, and divergence and divergence trend values that matched profiles with at least one LZP for the three different detection thresholds. The Kolmogorov-Smirnov tests showed that profiles with LZPs shallower than the MLD had significantly higher divergence values than the divergence values for all profiles for the 91^{st} ($p = 0.003$, $D^{+} = 0.073$), 95^{th} ($p << 0.0001$, $D^{+} = 0.135$) and 99^{th} ($p = 0.008$, $D^{+} = 0.153$) percentile (Figure 3.5). The Kolmogorov-Smirnov tests showed that profiles with LZP shallower than the MLD had significantly higher divergence trend than the divergence trend for all profiles for the 91^{st} ($p = 0.002$, $D^{+} = 0.077$), 95^{th} ($p << 0.0001$, $D^{+} = 0.143$) and 99^{th} ($p = 0.03$, $D^{+} = 0.131$) percentile (Figure 3.6).

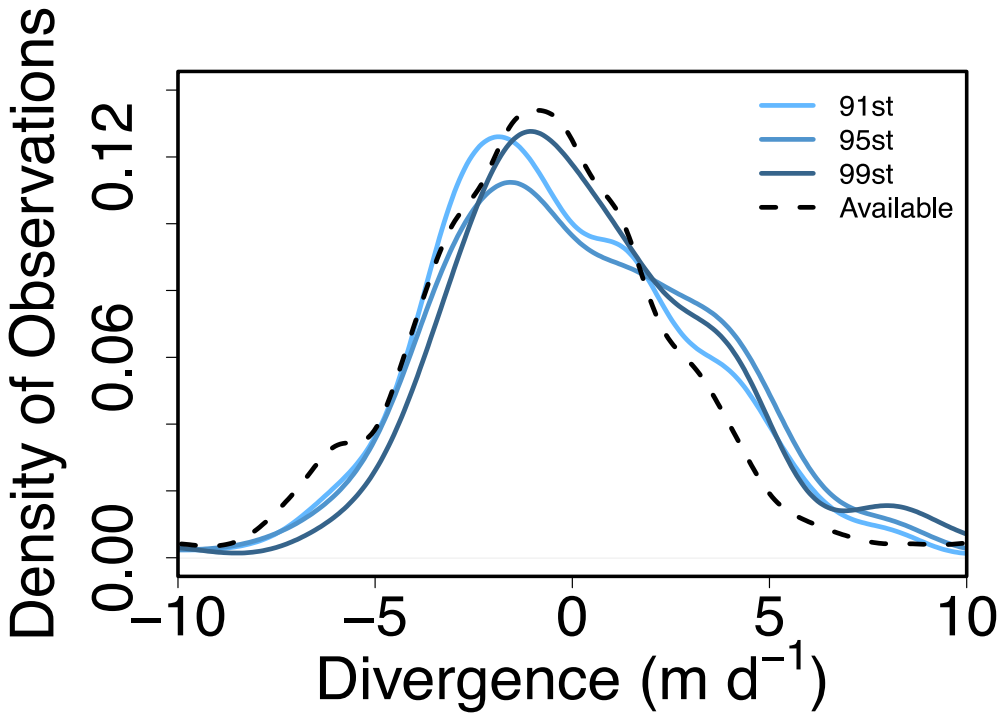

Figure 3.5: The distribution of all divergence values during the study (dashed line). Positive values indicate upward vertical velocities (divergence), and negative values indicate downward vertical velocities. The distributions of divergence values associated with the three LZP thresholds are solid blue lines. These lines are shifted toward more divergent vertical velocities.

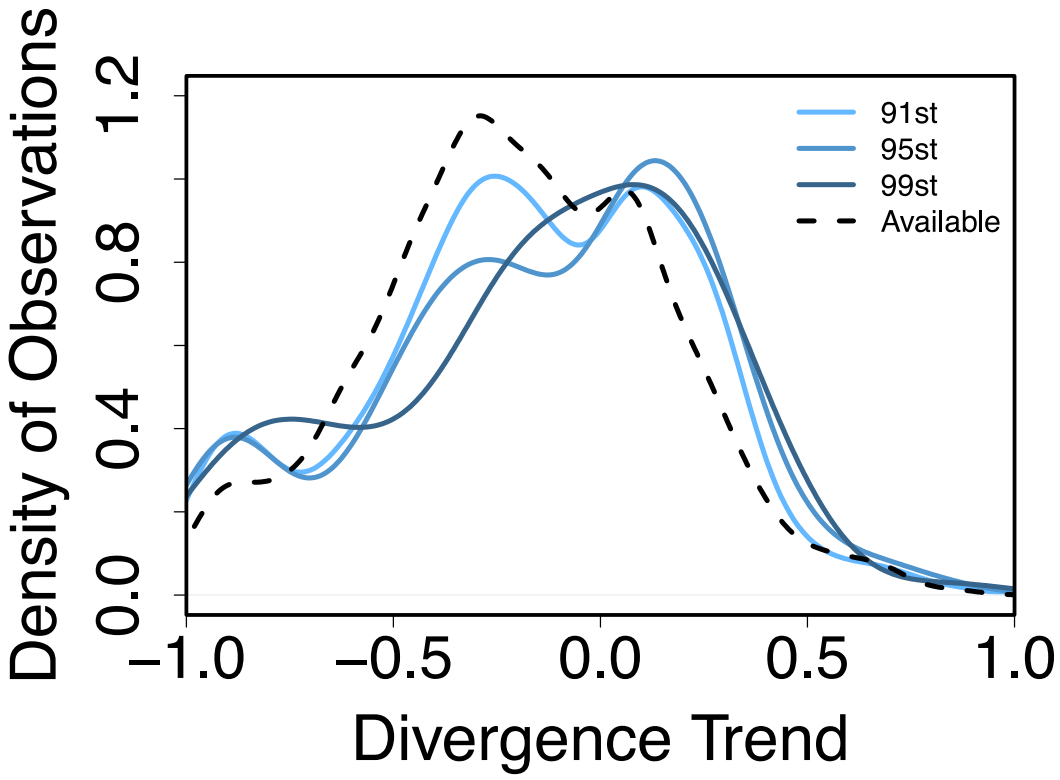

Figure 3.6: The distribution of all divergence trend values during the study (dashed line). Positive values indicate persistent upward vertical velocities (divergence), and negative values indicate persistent downward vertical velocities over 12 hours. The distributions of divergence trend values associated with the three LZP thresholds are solid blue lines. These lines are shifted toward more consistently divergent conditions.

Two generalized linear mixed models were used to test which Eulerian advection metrics combined with environmental factors were the most strongly associated with profiles with LZPs shallower than the mixed layer for the three different LZP thresholds. Since divergence and divergence trend were correlated (R = 0.35), it was not suitable to include both in the same model. Instead, separate models were developed that included divergence and divergence trend (Table 3.1, 3.2). For all three LZP thresholds, increased divergence and divergence trend values were

significantly more likely to have LZPs above the MLD, which means LZPs were more likely with higher divergence or divergence trend values. Sun angle was a significant negative predictor of LZPs for these two models, except for the 99th percentile threshold in the model including divergence trend (Table 3.2), which means more LZPs were above the mixed layer when the sun was low in the sky. Chlorophyll values were significantly lower in the models for the 91st and 95th, but not the 99th percentile threshold, while temperature values were significantly higher in the 95th and 99th, but not the 91st percentile threshold (Tables 3.1, 3.2). Tidal phase was not a significant predictor of LZPs. MLD was only significant for the 91st threshold for both these models. Conditional R^2 estimates were moderate for the 91st and 95th percentile thresholds, and low for the 99th percentile threshold. This likely reflects the reduced number of LZPs in the model for this high threshold. Notably, the effect of tide detected in figure 3.4 was not seen in these models.

Table 3.1: Estimates and Z-scores from a generalized linear mixed model including Eulerian divergence estimates. Bold values indicate $p < 0.05$.

LZP Thresh.		Div.	Sun Angle	Mean Chl.	Mean Temp.	Tide Phase (SD)	MLD	Cond. R^2
91%	Estimate	**0.063**	**-1.956**	**-0.084**	0.406	-0.524	**0.024**	0.338
	Z-score	**3.925**	**-9.322**	**-2.172**	1.552	-1.053	**2.546**	
95%	Estimate	**0.099**	**-1.269**	**-0.095**	**1.056**	-0.235	0.002	0.322
	Z-score	**5.304**	**-5.206**	**-2.178**	**3.310**	-0.395	0.171	
99%	Estimate	**0.093**	**-0.881**	-0.047	**1.708**	-0.861	-0.002	0.118
	Z-score	**3.212**	**-2.198**	-0.684	**2.925**	-1.201	-0.109	

Table 3.2: Estimates and Z-scores from a generalized linear mixed model including Eulerian divergence trend estimates. Bold values indicate $p < 0.05$.

LZP Thresh.		Div. Trend	Sun Angle	Mean Chl.	Mean Temp.	Tide Phase (SD)	MLD	Cond. R^2
91%	Estimate	**0.782**	**-1.854**	**-0.086**	0.433	-0.535	**0.027**	0.351
	Z-score	**3.642**	**-8.717**	**-2.176**	1.643	-1.039	**2.768**	
95%	Estimate	**1.052**	**-1.096**	**-0.092**	**1.094**	-0.219	0.007	0.339
	Z-score	**4.249**	**-4.413**	**-2.092**	**3.430**	-0.358	0.567	
99%	Estimate	**1.165**	-0.659	-0.040	**1.751**	-0.862	0.009	0.132
	Z-score	**2.980**	-1.625	-0.579	**3.002**	-1.159	0.447	

3.5 LZPs with Lagrangian metrics

Forward and backward FTLE values were calculated twice per day using a 12-hour particle tracing simulation starting at 0Z and 12Z. Forward FTLE values were estimated from particle simulations starting at 0Z and 12Z and tracked in forward time for 12 hours. Backward FTLE values were estimated from particle simulations tracked in backward time for 12 hours. Of the 3,320 profiles sampled, 504 profiles occurred during the restricted forward FTLE window at the end of the forward FTLE simulation (9-12Z, 21-24Z) for which I matched forward FTLE, sun angle, chlorophyll, temperature, tide phase, and MLD values. Of these profiles 142, 91, and 21 of them had LZPs above the MLD for the 91^{st}, 95^{th}, and 99^{th} percentile threshold, respectively. Of the 3,320 profiles sampled, 657 profiles occurred during the restricted backward FTLE window at the end of the backward FTLE simulation (0-3Z, 12-15Z) for which I have matched FTLE, sun angle, chlorophyll, temperature, tide phase, and MLD values. Of these profiles 162, 104, and 29 of them had LZPs above the MLD for the 91^{st}, 95^{th}, and 99^{th} percentile threshold, respectively.

To compare the effect forward and backward FTLE had on LZPs shallower than the MLD, I performed a Kolmogorov-Smirnov test between all forward and backward FTLE values matched to station keeping profiles and forward and backward FTLE values that matched profiles with at least one LZP for the three different detection thresholds. The Kolmogorov-Smirnov tests showed that profiles with LZP shallower than the MLD had significantly higher forward FTLE values than the forward FTLE values for all profiles for the 91^{st} ($p << 0.0001$, $D^{\wedge}+ = 0.20$), 95^{th} ($p << 0.0001$, $D^{\wedge}+ = 0.24$) and 99^{th} ($p = 0.0056$, $D^{\wedge}+ = 0.36$) percentile (Figure 3.7). The Kolmogorov-Smirnov tests showed that profiles with LZP shallower than the MLD

had significantly higher backward FTLE values than the backward FTLE values for all profiles for the 91st (p = 0.04, D^+ = 0.11), 95th (p = 0.0002, D^+ = 0.217) and 99th (p = 0.012, D^+ = 0.28) percentile (Figure 3.8).

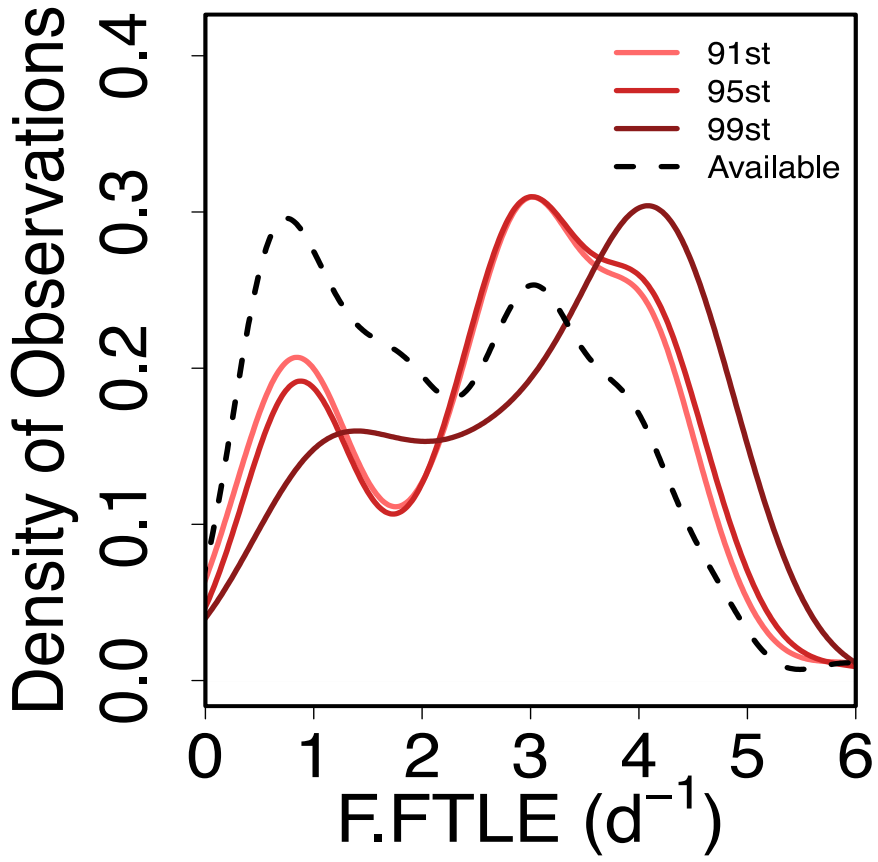

Figure 3.7: The distribution of all forward FTLE values during the study (dashed line). Higher values indicate more diffluent conditions. The distributions of forward FTLE values associated with the three LZP thresholds are solid red lines. These lines are shifted toward more diffluent conditions.

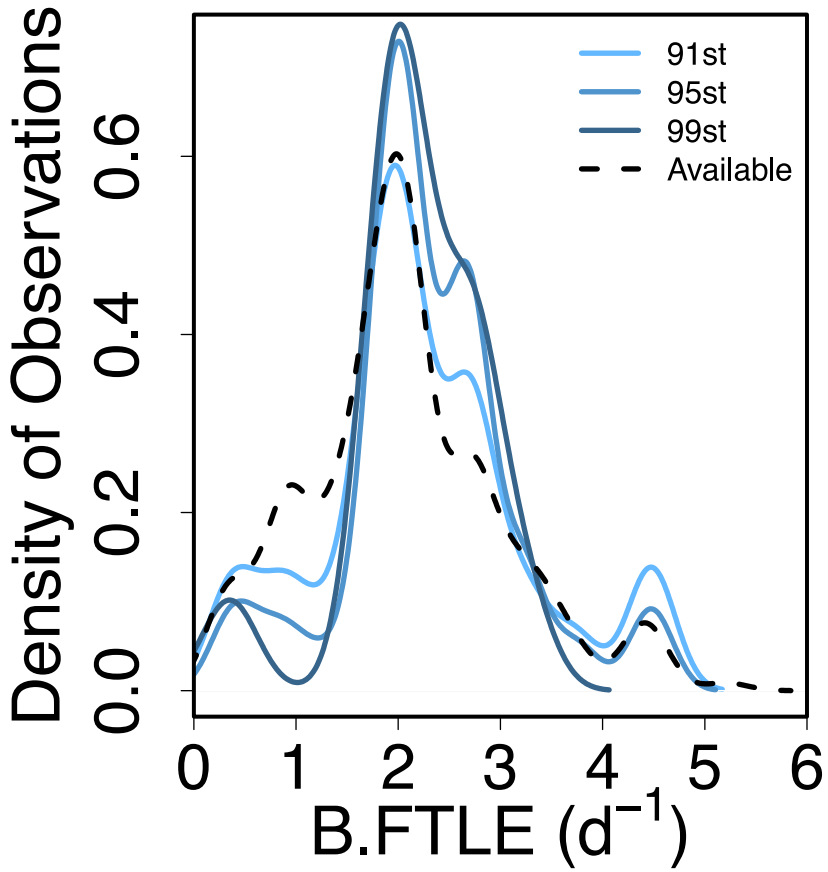

Figure 3.8: The distribution of all backward FTLE values during the study (dashed line). Higher values indicate more confluent conditions. The distributions of backward FTLE values associated with the three LZP thresholds are solid blue lines. These lines are shifted toward more confluent conditions.

Four generalized linear mixed models were used to test which Lagrangian advective metrics and environmental factors were the most strongly associated with profiles with LZPs shallower than the mixed layer for the three different LZP thresholds. Since the data match ups for the forward and backward FTLE values did not occur at the same time period, I ran separate models for each of these. Additionally, I created two additional models that thresholded the forward and

backward FTLE values into the presence or absence of LCS. RLCS were considered present for forward FTLE values greater than the median forward FTLE value. ALCS were considered present for backward FTLE values greater than the median backward FTLE value.

For all three LZP thresholds, increased forward FTLE values were significantly more likely to have profiles with LZPs above the MLD, which means LZPs were more likely with higher forward FTLE values. Sun angle was a significant predictor of LZPs for the 91st and 95th percentile threshold, both showing a strong negative effect, which means more LZPs were above the mixed layer when the sun was low in the sky. Mean chlorophyll above the mixed layer was only significant for the 91% threshold, showing a negative effect, and mean temperature was significant for 95% threshold, showing a positive effect. All other predictors were non-significant (Table 3.3). The model results for thresholded forward FTLE (Table 3.4), which were used to identify the presence and absence of potential rLCS are highly similar to the model results with non-thresholded forward FTLE values (Table 3.3).

Table 3.3: Estimates and Z-scores from a generalized linear mixed model including Lagrangian forward FTLE estimates. Bold values indicate $p < 0.05$.

LZP Thresh.		F. FTLE	Sun Angle	Mean Chl.	Mean Temp.	Tide Phase (SD)	MLD	Cond. R^2
91%	Estimate	**0.440**	**-3.437**	**-0.219**	0.692	-0.501	0.006	0.386
	Z-score	**3.861**	**-2.754**	**-2.337**	1.325	-0.826	0.323	
95%	Estimate	**0.511**	**-3.297**	-0.187	**1.298**	-0.288	-0.011	0.394
	Z-score	**3.820**	**-2.310**	-1.769	**2.120**	-0.442	-0.505	
99%	Estimate	**0.670**	0.278	-0.051	1.106	-1.482	-0.001	0.008
	Z-score	**2.552**	0.109	-0.263	0.950	-1.494	-0.036	

Table 3.4: Estimates and Z-scores from a generalized linear mixed model including thresholded Lagrangian forward FTLE estimates. Bold values indicate $p < 0.05$.

LZP Thresh.		F.FTLE (Low)	Sun Angle	Mean Chl.	Mean Temp.	Tide Phase (SD)	MLD	Cond. R^2
91%	Estimate	**-1.361**	**-3.425**	**-0.215**	0.653	-0.749	0.007	0.418
	Z-score	**-4.559**	**-2.699**	**-2.264**	1.257	-1.206	0.344	
95%	Estimate	**-1.576**	**-3.248**	-0.177	**1.249**	-0.573	-0.008	0.447
	Z-score	**-4.311**	**-2.239**	-1.653	**2.033**	-0.835	-0.383	
99%	Estimate	**-1.513**	0.316	-0.041	1.167	-1.673	0.005	0.004
	Z-score	**-2.148**	0.124	-0.208	0.961	-1.601	0.130	

For all three LZP thresholds, backward FTLE values were not significant predictors of LZP above the mixed layer. For this model only negative sun angle for the 91st and 95th percentile significantly predicted LZPs, while MLD only significantly predicted LZPs for the 91st percentile (Table 3.5). The model results for thresholded backward FTLE, which were used to identify the presence and absence of potential aLCS are highly similar to the model results with non-thresholded backward values (Table 3.6). Conditional R^2 estimates were moderate for the 91st and 95th percentile thresholds for these models, and low for the 99th percentile threshold. This likely reflects the reduced number of LZPs in the model for this high threshold. Notably, the effect of tide detected in figure 3.4 was not seen in these models.

Table 3.5: Estimates and Z-scores from a generalized linear mixed model including Lagrangian backward FTLE estimates. Bold values indicate $p < 0.05$.

LZP Thresh.		B.FTLE	Sun Angle	Mean Chl.	Mean Temp.	Tide Phase (SD)	MLD	Cond. R^2
91%	Estimate	-0.117	**-1.586**	0.034	0.218	-0.828	**0.038**	0.452
	Z-score	-0.749	**-3.504**	0.410	0.462	-1.171	**2.172**	
95%	Estimate	0.129	**-1.214**	0.059	-0.115	-0.432	0.013	0.430
	Z-score	0.701	**-2.295**	0.622	-0.215	-0.568	0.683	
99%	Estimate	0.107	-1.226	0.076	0.078	-0.393	-0.011	0.003
	Z-score	0.412	-1.548	0.603	0.110	-0.587	-0.415	

Table 3.6: Estimates and Z-scores from a generalized linear mixed model including thresholded Lagrangian backward FTLE estimates. Bold values indicate $p < 0.05$.

LZP Thresh.		B.FTLE (Low)	Sun Angle	Mean Chl.	Mean Temp.	Tide Phase (SD)	MLD	Cond. R^2
91%	Estimate	-0.079	**-1.466**	0.037	0.198	-0.904	**0.035**	0.428
	Z-score	-0.252	**-3.300**	0.448	0.427	-1.315	**2.045**	
95%	Estimate	-0.407	**-1.179**	0.057	-0.120	-0.546	0.013	0.419
	Z-score	-1.131	**-2.251**	0.601	-0.224	-0.723	0.658	
99%	Estimate	-0.664	-1.130	0.076	0.135	-0.589	-0.012	0.012
	Z-score	-1.297	-1.421	0.604	0.187	-0.853	-0.458	

Chapter 4

DISCUSSION

The observation that zooplankton are highly patchy is well known (Pinel-Alloul 1995; Folt & Burns 1999; Martin 2003). They typically show much higher variability at all length scales compared to phytoplankton (Mackas & Boyd 1979). Their high degree of variability is attributed to their interaction with phytoplankton (Levin 1992), internal waves (Wiebe et al. 1996; McManus et al. 2005), vertical migration (Cohen & Forward 2009; Zaret & Suffern 1976; Lampert 1989), and horizontal advection (Hofmann & Murphy 1999). Diel vertical migration is a ubiquitous feature of zooplankton communities. However, the intensity, pattern and vertical layering characteristics of these migrations can be taxa specific (Brierley et al. 1998). Figure 3.3 shows different intensities of DVM for the three different LZP thresholds. In each case, LZPs were significantly higher in shallow depths during nighttime hours, coincident with the prevailing mixed layer depth range (10-40m). However, the DVM patterns were not identical for each threshold. While the presence of DVM gives strong circumstantial evidence that our method is detecting the local zooplankton community, it is likely that our thresholds are selecting different members of the zooplankton community (Stanton et al. 1994), and therefore should be interpreted with caution. The presence of LZPs above the mixed layer was consistently significantly related to negative sun angle for the 91^{st} and 95^{th} threshold values (Tables 3.1-3.6). An increased probability of zooplankton presence is associated with nighttime when the sun was low in the sky. However, the 99^{th} percentile threshold was

only significantly related to sun angle in table 3.1. This is consistent with Figure 3.3C, which shows that this threshold had the lowest intensity of DVM. This signal was not far removed from the mixed layer depth, which was also coherent with higher concentrations of phytoplankton over the entire water column (Figure 3.2C). This may show that these organisms are balancing the predator avoidance benefits of DVM with their needs for food resources (Cohen & Forward 2009).

Consistent with previous findings of (Bernard & Steinberg 2013; Bernard et al. 2017; Oliver et al. 2013), tidal regime was related to the presence of LZPs above the mixed layer. For all three LZP thresholds, there was a higher percent of presences above the mixed layer during diurnal tidal regimes than during semi-diurnal regimes (Figure 3.4). For the 91st and 95th LZP thresholds, the difference was significant. However, tidal regime was not a significant predictor in the GLMM models, indicating that the effect of tidal regime could be bound up in another predictor in the model. Also, there were almost three times as many glider profiles completed during semi-diurnal tides than diurnal tides; the number of observations during diurnal tides is a potential limitation of this study. Based on these results and coherent results in this area, I suggest that the tidal effect is aliased by other predictors in the model.

Analysis of the relationship between LZPs and Eulerian estimates of divergence and divergence trend showed that LZPs were found more often in positive divergence values (Figures 3.5, 3.6; Tables 3.1, 3.2). Positive values are indicative of local upwelling, which may transport phytoplankton from the lower mixed layer to the surface and be attractive for LZPs. Similarly, Lagrangian estimates of particle confluence and diffluence showed that LZPs were found more often in highly diffluent FTLEs and rLCS. Only the KS test with backward (confluent) FTLE values suggested

that LZPs were in convergent-like structures. However, this effect was not strong enough to be resolved in the GLMMs. Taken together these results suggest that higher diffluent (forward) FTLE values were related to increased probability of encountering zooplankton shallower than the MLD. This suggests that zooplankton in this region are resisting being advected as nearly passive particles, and that their swimming behavior may play a significant factor in both their vertical and horizontal distributions.

While I could not taxonomically partition the zooplankton community given the acoustic frequency I used in this study, Antarctic krill are a domination zooplankton species in the region (Ross et al. 2008; Ashjian et al. 2004; Lascara et al. 1999) and are likely included in our signal. Antarctic krill (*Euphausia superba*) are an important component considered to be a "keystone species" of the Southern Ocean (Quetin & Ross 1991). Krill are relatively large (1-3 cm) and are the primary food source for multiple species of baleen whales, seals, and penguins. Krill are major grazers of phytoplankton and prey on smaller zooplankton species (Price et al. 1988). Like other zooplankton, krill perform DVM in both winter and summer (Taki et al. 2005), but they are also good swimmers, able to sustain swimming speeds of 15 cm s^{-1} (Kils 1981) and maintain their position in the water allowing them to form aggregations (Hamner et al. 1983; Zhou & Dorland 2004). This means that their horizontal patterns can be determined both by behavior and current flows. Krill are thought to complete horizontal migrations to/from the coastal area to the continental shelf (Siegel 1988). The horizontal patchiness of krill is also reflected in the behaviors of krill predators, which dramatically change their movements around these patches. For example, humpback whales will switch to an area restricted search (Friedlaender

et al. 2013), while penguins will change their diving characteristics in a krill patch (Ainley 2002), indicating that the patchiness of prey resources heavily influences the movement ecology of these predators.

Most studies using LCS as an ecological cue only examine the confluent, aLCS features (Harrison et al. 2013; d'Ovidio et al. 2010; Maps et al. 2015; Tew Kai et al. 2009; Cotte et al. 2011; Della Penna et al. 2015). The underlying assumption in these studies is that horizontal advection dominates the horizontal distribution of prey fields (including zooplankton), thus are ecologically important to higher trophic levels. I am only aware of two studies that examined the influence of both diffluent and confluent Lagrangian metrics (Tew Kai et al. 2009; Harrison et al. 2013). One of these studies showed that Great Frigatebirds aggregated on both aLCS and rLCS. The second study was based on simulated zooplankton (isotropically swimming fish larvae) in aLCS and rLCS, and found that both structures had increased zooplankton concentrations compared to the background.

In our study, I found that divergent, diffluent, and rLCS features had higher zooplankton presences, and that convergent, confluent and aLCS were not predictors of zooplankton presence, which is different than the expectation given the previous studies focus on aLCS as possible aggregators of plankton and their predators. Admittedly, previous studies on phytoplankton, zooplankton and vertebrates were on much larger spatial scales O(100 km) compared to the ~500 m scale presented here, therefore the ecological significance of these structures may be quite different. Interestingly, the presence of LZPs were associated with lower mean chlorophyll values and either divergent (Tables 3.1, 3.2) or diffluent conditions (Tables 3.3, 3.4). One interpretation is that phytoplankton are being physically transported away from

these conditions, thus have lower concentrations. Alternatively, the depressed chlorophyll values could be a result of grazing by LZPs. GLMM models with mean chlorophyll as the response, and divergence or divergence trend as predictors, showed that mean chlorophyll above the mixed layer was higher in divergent areas (Table 4.1). GLMM models with forward or backward FTLE values as predictors of mean chlorophyll were inconclusive. This may suggest that transport away from divergent areas may not be the explanation for lower chlorophyll values associated with the presence of LZPs, and that grazing may be an explanation for lower chlorophyll values.

Table 4.1: Estimates and t-values from a generalized linear mixed model for the relationship between Divergence and Divergence trend and mean chlorophyll above the mixed layer.

		Divergence	Divergence Trend	Cond. R^2
Mean Chlorophyll	Estimate	**0.002**		0.440
	t-value	**2.104**		
Mean Chlorophyll	Estimate		**0.562**	0.437
	t-value		**3.904**	

The distribution of zooplankton can be attributed to advection or behavior, making the distribution of these organisms challenging to understand. I considered both mechanisms with respect to the results from this study. The strong DVM pattern that I see suggests that behavior is the primary driver of vertical movement. Horizontal mechanisms influencing LZP presence are less clear. If advective forces were the primary driver of LZP distribution I would expect to see convergent (negative divergence and divergence trend values), confluent (backward FTLE), and aLCS features as significant predictors of LZP, but that is not evident in our analysis. It is

tempting to attribute higher concentrations of chlorophyll to the possible localized upwelling of nutrients that then drive localized phytoplankton growth. This is a common framework for understanding higher phytoplankton concentrations in divergent, upwelling systems at large scales. However, I do not think this is likely the case since the residence time in the surface waters over Palmer Canyon is ~ 2 days (Kohut et al. 2018), which is much shorter than the scale of locally measured phytoplankton growth rates (Moline 1996). Instead, it is possible that there are behavioral and taxonomic explanations for higher chlorophyll concentrations on divergent fronts.

Franks 1992 used a model of two dimensional flow and variable swimming speeds to show how weakly swimming planktonic organisms could accumulate on divergent fronts. In this case, weak swimmers were defined as swimmers small enough and slow enough to be transported by vertical velocities, such as small flagellated phytoplankton (5-20 μm). This study showed that the weak swimming velocities resulted in higher concentrations of weak swimmers across isopycnals in divergent flows. This is significant because the dominant phytoplankton types in January and February at Palmer Station are not diatoms, but small flagellated phytoplankton including cryptophytes, prymnesiophytes and chlorophytes (Moline & Prézelin 1996). Therefore, in the Eulerian framework, there may be a phytoplankton behavioral explanation for increased chlorophyll at divergent fronts that could then attract zooplankton grazers. However, more work is necessary to confirm this hypothesis.

In this study I attempt to understand both behavioral and advective factors that drive zooplankton distributions in Palmer Canyon, Antarctica. I find that vertical

migration is a strong signal, and unexpectedly, that these zooplankton were found in divergent and diffluent advective features. This suggests that zooplankton behavior may be important in understanding both their vertical and horizontal distributions in this region.

REFERENCES

Ainley, D (2002) The Adélie penguin: bellwether of climate change, Columbia University Press, New York

Ashjian, CJ Rosenwaks, GA Wiebe, PH Davis, CS and others (2004) Distribution of zooplankton on the continental shelf off marguerite bay, antarctic peninsula, during austral fall and winter, 2001. Deep Sea Research Part II: Topical Studies in Oceanography 51:2073–2098

Atkinson, A (1998) Life cycle strategies of epipelagic copepods in the southern ocean. Journal of Marine Systems 15:289–311

Barrick, DE Evans, MW, Weber, BL (1977) Ocean surface currents mapped by radar. Science 198:138−144

Bartoń, K (2017) Mumin: Multi-model inference. R package version 1.40.0

Baumgartner, MF, Fratantoni, DM (2008) Diel periodicity in both sei whale vocalization rates and the vertical migration of their copepod prey observed from ocean gliders. Limnology and …

Bernard, KS, Steinberg, DK (2013) Krill biomass and aggregation structure in relation to tidal cycle in a penguin foraging region off the Western Antarctic Peninsula. ICES Journal of Marine Science 70:834–849

Bernard, KS Cimino, M Fraser, W Kohut, J and others (2017) Factors that affect the nearshore aggregations of Antarctic krill in a biological hotspot. Deep Sea Research Part I: Oceanographic Research Papers 126:139–147

Brierley, AS Ward, P Watkins, JL, Goss, C (1998) Acoustic discrimination of southern ocean zooplankton. Deep-Sea Research II 45:1155–1173

Carvalho, F Kohut, J Oliver, MJ, Schofield, O (2017) Defining the ecologically relevant mixed-layer depth for Antarctica's coastal seas: Mid in coastal Antarctica. Geophys Res Lett 44:338–345

Catton, KB Webster, DR Kawaguchi, S, Yen, J (2011) The hydrodynamic disturbances of two species of krill: Implications for aggregation structure. J Exp Biol 214:1845

Chojnacki, J, Węgleńska, T (1984) Periodicity of composition, abundance, and vertical distribution of summer zooplankton (1977/1978) in Ezcurra Inlet, admiralty bay (King George Island, South Shetland). J Plankton Res 6:997–1017

Cimino, MA Moline, MA Fraser, WR Patterson-Fraser, DL, Oliver, MJ (2016) Climate-driven sympatry may not lead to foraging competition between congeneric top-predators. Sci Rep 6:18820

Cohen, JH, Forward, RB (2009) Zooplankton diel vertical migration – a review of proximate control. Oceanography and marine biology: an annual review. CRC Press, Boca Raton, pp 77–110

Cotte, C D'ovidio, F Chaigneau, A Lèvy, M Taupier-Letage, I Mate, B, Guinet, C (2011) Scale-dependent interactions of Mediterranean whales with marine dynamics. Limnol Oceanogr 56:219–232

Croll, DA Marinovic, B Benson, S Chavez, FP Black, N Ternullo, R, Tershy, BR (2005) From wind to whales trophic links in a coastal upwelling system. Marine Ecology Progress Series 289:117–130

D'ovidio, F De Monte, S Alvain, S Dandonneau, Y, Levy, M (2010) Fluid dynamical niches of phytoplankton types. Proceedings of the National Academy of Sciences 107:18366–18370

Della Penna, A De Monte, S Kestenare, E Guinet, C, D'ovidio, F (2015) Quasi-planktonic behavior of foraging top marine predators. Sci Rep 5:18063

Dzwonkowski, B Lipphardt, BL Kohut, JT Yan, X-H, Garvine, RW (2010) Synoptic measurements of episodic offshore flow events in the central Mid-Atlantic bight. Continental Shelf Research 30:1373–1386

Emslie, SD Fraser, W Smith, RC, Walker, W (1998) Abandoned penguin colonies and environmental change in the palmer station area, Anvers Island, Antarctic peninsula. Antarctic Science 10

Folt, CL, Burns, CW (1999) Biological drivers of zooplankton patchiness. Trends in Ecology & Evolution 14:300–305

Franks, PJS (1992) Sink or swim: Accumulation of biomass at fronts. Marine Ecology Progress Series 82:1–12

Friedlaender, AS Fraser, WR Patterson, D Qian, SS, Halpin, PN (2008) The effects of prey demography on humpback whale (megaptera novaeangliae) abundance around Anvers Island, Antarctica. Polar Biol 31:1217–1224

Friedlaender, AS Tyson, RB Stimpert, AK Read, AJ, Nowacek, DP (2013) Extreme diel variation in the feeding behavior of humpback whales along the western Antarctic peninsula during autumn. Mar Ecol Prog Ser 494:281–289

Gong, D Kohut, JT, Glenn, SM (2010) Seasonal climatology of wind-driven circulation on the New Jersey shelf. J Geophys Res 115:389

Haller, G (2015) Lagrangian coherent structures. Annu Rev Fluid Mech 47:137–162

Hamner, WM Hamner, PP Strand, SW, Gilmer, RW (1983) Behavior of Antarctic krill, euphausia superba: Chemoreception, feeding, schooling, and molting. Science 220:433–435

Harrison, CS Siegel, DA, Mitarai, S (2013) Filamentation and eddy−eddy interactions in marine larval accumulation and transport. Mar Ecol Prog Ser 472:27–44

Hofmann, EE, Murphy, EJ (1999) Advection, krill, and Antarctic marine ecosystems. Antarctic Science 16:487–499

Kavanaugh, MT Abdala, FN Ducklow, H Glover, D and others (2015) Effect of continental shelf canyons on phytoplankton biomass and community composition along the western Antarctic peninsula. Mar Ecol Prog Ser 524:11–26

Kavanaugh, MT Oliver, MJ Chavez, FP Letelier, RM Muller-Karger, FE, Doney, SC (2016) Seascapes as a new vernacular for pelagic ocean monitoring, management and conservation. ICES Journal of Marine Science 73:1839–1850

Kils, U (1981) Swimming behaviour, swimming performance and energy balance of antarctic krill euphausia superba. BIOMASS Scientific Series No. 3:122

Kohut, J Bernard, K Fraser, W Oliver, MJ Statscewich, H Winsor, P Miles, T (2014) Studying the Impacts of Local Oceanographic Processes on Adélie Penguin Foraging Ecology. Marine Technology Society Journal 48(5):25-34.

Kohut, JT Winsor, P Statscewich, H Oliver, MJ and others (2018) Variability in summer surface residence time within a western Antarctic Peninsula biological hotspot. Philosophical Transactions of the Royal Society

Kuznetsova, A Brockhoff, PB, Christensen, RHB (2016) Lmertest: Tests in linear mixed effects models. R package version 2:0–33

Lampert, W (1989) The adaptive significance of diel vertical migration of zooplankton. Functional Ecology 3:21–27

Lascara, CM Hofmann, EE Ross, RM, Quetin, LB (1999) Seasonal variability in the distribution of antarctic krill, euphausia superba, west of the antarctic peninsula. Deep Sea Research Part I: Oceanographic Research Papers 46:951–984

Lawson, GL Wiebe, PH Ashjian, CJ Gallager, SM Davis, CS, Warren, JD (2004) Acoustically-inferred zooplankton distribution in relation to hydrography west of the Antarctic Peninsula. Deep Sea Research Part II: Topical Studies in Oceanography 51:2041–2072

Levin, SA (1992) The problem of pattern and scale in ecology: The Robert h. Macarthur award lecture. Ecology 73:1943–1967

Lohrmann, A (2001) Monitoring sediment concentration with acoustic backscattering instruments. Nortek Technical Note 3

Mackas, DL, Boyd, CM (1979) Spectral analysis of zooplankton spatial heterogeneity. Science 204:62–64

Maps, F Plourde, S Mcquinn, IH St-Onge-drouin, S Lavoie, D Chasse□, J, Lesage, V (2015) Linking acoustics and finite-time lyapunov exponents reveals areas and mechanisms of krill aggregation within the gulf of St. Lawrence, eastern Canada. Limnology and Oceanography 60:1965–19755

Martin, AP (2003) Phytoplankton patchiness: The role of lateral stirring and mixing. Progress in Oceanography 57:125–174

Mcmanus, MA Cheriton, OM Drake, PJ Holliday, DV Storlazzi, CD Donaghay, PL, Greenlaw, CF (2005) Effects of physical processes on structure and transport of thin zooplankton layers in the coastal ocean. Mar Ecol Prog Ser 301:199–215

Melville, WK (1996) The role of surface-wave breaking in air-sea interaction. Annu Rev Fluid Mech 28:279–321

Moline, MA (1996) Temporal dynamics and regulation of coastal Antarctic phytoplankton communities: Spring/summer 1991-1994. University of California, Santa Barbara

Moline, MA, Prézelin, BB (1996) Long-term monitoring and analyses of physical factors regulating variability in coastal Antarctic phytoplankton biomass, in situ productivity and taxonomic composition over subseasonal, seasonal and interannual time scales. Marine Ecology Progress Series 145:143–160

Oliver, MJ Irwin, A Moline, MA Fraser, W Patterson, D Schofield, O, Kohut, J (2013) Adélie penguin foraging location predicted by tidal regime switching. PLoS One 8:e55163

Paduan, JD, Graber, HC (1997) Introduction to high-frequency radar: Reality and myth. Oceanography 10:36–39

Paffenhöfer, G-A (1980) Zooplankton distribution as related to summer hydrographic conditions in Onslow Bay, North Carolina. Bulletin of Marine Science 30:819–832

Palamara, L Manderson, J Kohut, J Oliver, MJ Gray, S, Goff, J (2012) Improving habitat models by incorporating pelagic measurements from coastal ocean observatories. Marine Ecology Progress Series 447:15–30

Pinel-Alloul, P (1995) Spatial heterogeneity as a multiscale characteristic of zooplankton community. Hydrobiologia 300:17-42

Price, HJ Boyd, KR, Boyd, CM (1988) Omnivorous feeding behavior of the Antarctic krill Euphausia superba. Mar Biol 97:67–77

Quetin, LB Ross, RM (1991) Behavioral and physiological characteristics of the Antarctic krill, Euphausia superba. American Zoologist

Roe, HSJ Griffiths, G (1993). Biological information from an acoustic Doppler current profiler. Mar Biol 115:339-346.

Ross, RM Quetin, LB Martinson, DG Iannuzzi, RA Stammerjohn, SE, Smith, RC (2008) Palmer lter: Patterns of distribution of five dominant zooplankton species in the epipelagic zone west of the Antarctic Peninsula, 1993–2004. Deep Sea Research Part II: Topical Studies in Oceanography 55:2086–2105

Russell, RW Harrison, NM, Hunt, GL (1999) Foraging at a front: Hydrography, zooplankton, and avian planktivory in the northern Bering Sea. Marine Ecology Progress Series 182:77–93

R Core Team (2017) R: A language and environment for statistical computing. R Foundation for Statistical Computing

Schnack-Schiel, SB, Mujica, A (1994) The zooplankton of the Antarctic Peninsula region. Southern Ocean ecology. The BIOMASS perspective. pp 79–92

Siegel, V (1988) A Concept of Seasonal Variation of Krill (Euphausia superba) Distribution and Abundance West of the Antarctic Peninsula. In: Sahrhage, D (ed) A Concept of Seasonal Variation of Krill (Euphausia superba) Distribution and Abundance West of the Antarctic Peninsula, Antarctic Ocean and Resources Variability. Springer Berlin Heidelberg, Berlin, Heidelberg, pp 219–230

Simard, Y De Ladurantaye, R, Therriault, J-C (1986) Aggregation of euphausiids along a coastal shelf in an upwelling environment. Marine Ecology Progress Series 32:203–215

Smith, RC Baker, KS Fraser, WR Hofmann, EE, Karl, DM (1995) The Palmer LTER: A long-term ecological research program at palmer station, Antarctica. …

Stanton TK, Wiebe PH, Chu D, Benfield MC, Scanlon L, Martin L, Eastwood RL (1994) On acoustic estimates of zooplankton biomass. ICES Journal of Marine Science 51:505-12.

Taki, K Hayashi, T, Naganobu, M (2005) Characteristics of seasonal variation in diurnal vertical migration and aggregation of Antarctic krill (euphausia superba) in the scotia sea, using Japanese fishery data. CCAMLR Science 12:163–172

Tew Kai, E Rossi, V Sudre, J Weimerskirch, H and others (2009) Top marine predators track lagrangian coherent structures. Proc Natl Acad Sci U S A 106:8245–8250

Wiebe, PH Mountain, DG Stanton, TK Greene, CH and others (1996) Acoustical study of the spatial distribution of plankton on Georges Bank and the relationship between volume backscattering strength and the taxonomic composition of the plankton. Deep Sea Research Part II: Topical Studies in Oceanography 43:1971–2001

Wishner, KF Schoenherr, JR Beardsley, R, Chen, C (1995) Abundance, distribution and population structure of the copepod calanus finmarchicus in a springtime right whale feeding area in the southwestern Gulf of Maine. Continental Shelf Research 15:475–507

Yen, J (2000) Life in transition: Balancing inertial and viscous forces by planktonic copepods. The Biological Bulletin 198:213–224

Zaret, TM, Suffern, JS (1976) Vertical migration in zooplankton as a predator avoidance mechanism. Limnol Oceanogr 21:804–813

Zhou, M Nordhausen, W, Huntley, M (1994) Adcp measurements of the distribution and abundance of euphausiids near the Antarctic Peninsula in winter. Deep Sea Research I 41:1425–1445

Zhou, M, Dorland, RD (2004) Aggregation and vertical migration behavior of euphausia superba. Deep Sea Research Part II: Topical Studies in Oceanography 51:2119–2137